Topological Representations for Data Analysis : Use Cases on Instabilities and Turbulences

Fabien Vivodtzev[1,*], *Florent* Nauleau[1,**], *Alexis* Casner[1,***], and *Julien* Tierny[2,****]

[1]CEA/CESTA,
[2]Sorbonne Université, CNRS

Abstract. Understanding physical phenomena implied in the design of a system or in the guarantee of its performances require to run high fidelity simulation codes and to create experimental campaigns at different scales. Thanks to the use of advanced sensors or imaging capabilities in large facilities such as the Laser Mega Joule and the use of High Performance Computing, very large and complex dataset are generated. The analysis of such data is a real challenge due to the size and the complexity of the data. When dealing with chaotic phenomena, traditional analysis methods often try to average the answer. In this paper, we introduce the use of Topological Data Analysis (TDA) to improve the understanding of the results and avoid costly traditional analysis methods. The key concepts of TDA are presented such as the notion of critical points, persistence and different simplification representations. Then we illustrate the advantages of TDA on successful use cases on the analysis of hydrodynamic instabilities observed during Laser shooting or turbulences computed with a computational fluid dynamic simulation code.

1 Analysis of large and complex data

To design, optimize or guarantee the performance of a system, large-scale simulations in various fields such as plasma physics, electromagnetism and aerodynamics are carried out at CEA. The use of High Performance Computing approaches to run the simulation codes and advanced sensors capabilities lead to the generation of very large and complex dataset that scientists need to explore to understand the physical phenomena. Traditional analysis approaches based on scientific imaging (*e.g.* L_2 norm) or feature segmentation (*e.g.* watershed) can be challenging to apply effectively to chaotic phenomena. The purpose of this work is to introduce an alternative analysis approach in order to help the scientists understand their complex and large data.

1.1 Topological representations

At the interface between Mathematics and Computer Science, Topological Data Analysis (TDA) [1] forms a family of generic, robust and efficient techniques to analyze complex

---

*e-mail: fabien.vivodtzev@cea.fr
**e-mail: florent.nauleau@cea.fr
***e-mail: alexis.casner@cea.fr
****e-mail: julien.tierny@sorbonne-universite.fr

features in scientific data. TDA helps to identify hidden features in the structure of the data and ease the comparison in ensembles [2]. More precisely, Persistent Homology [3] measures topological features of shapes and of functions by tracking topological changes of a changing space. This approach has been successfully used in various fields such as in medical imaging [4], combustion [5] or astrophysics [6].

1.2 Related work in Topological Data Analysis

Concepts and algorithms from computational topology have been investigated, adapted and extended by the visualization community for decades [7]. The classification of topological methods can be expressed depending on the dimension of the input data such as a scalar, vector or tensor and its evolution over time. A substantial corpus of literature [8] has been dedicated to the visualization of flow data with topological methods. However, in many applications, the features of interest can be reliably represented by considering a single pointwise scalar descriptor, such as pressure or intensity for instance. Such a transition to a scalar descriptor enables users to leverage the ensemble of existing tools for scalar data analysis. For example a single pixel information based on post-processing of radiographic images can be sufficient to study instabilities during the ignition phase [9]. In computational fluid dynamic, a relevant scalar descriptor can be sufficient to study the evolution of the vorticity structure [10].

Many topological representations have been introduced for scalar data. For example the persistence curve and the persistence diagram [1] can help represent the population of features of interest in function of their salience. Different representations of segmentation can be manipulated such as the merge trees [11] or the Morse-Smale complex [12], which depicts the global behavior of integral lines. Robust and efficient algorithms have been introduced for the computation of the Morse-Smale complex based on discrete Morse theory [13]. Comparison of ensemble dataset is an important step of the analysis. This is why various metrics between topological descriptors have been proposed [14]. Based on a bipartite assignment problem, the Wasserstein distance [1] between ensembles has been extensively used. It enables users to compare ensemble members directly based on their topological representation such as persistence diagrams or merge trees.

2 Introduction to Topological Data Analysis

This section introduces the key concepts of Topological Data Analysis which are used to build our visualization pipelines. Readers interested in TDA are encouraged to refer to the formal introduction provided in [1]. These concepts are used at CEA through the design of visualization pipelines starting from data preparation at the simulation code level or through postprocessing tools after the data has been generated. Then the Paraview software [15] is mainly used because it allows large data visualizations. Thanks to the *Topology ToolKit (TTK)* [16] most of the topological representations needed in these studies are directly available and integrated to Paraview.

2.1 Input data

In order to apply topological tools the input data is represented as an ensemble of *N piecewise linear scalar fields* $f_i : \mathcal{M} \rightarrow \mathbb{R}$, with $i \in \{1, \ldots, N\}$, defined on a piecewise linear d-manifold $\mathcal{M}$, with $d = 2$ in this paper. A triangulation is given on the domain with a simplicial complex. The scalar values are given at the vertices of $\mathcal{M}$ and are linearly interpolated on the simplices of higher dimensions as shown on Figure 1 (b).
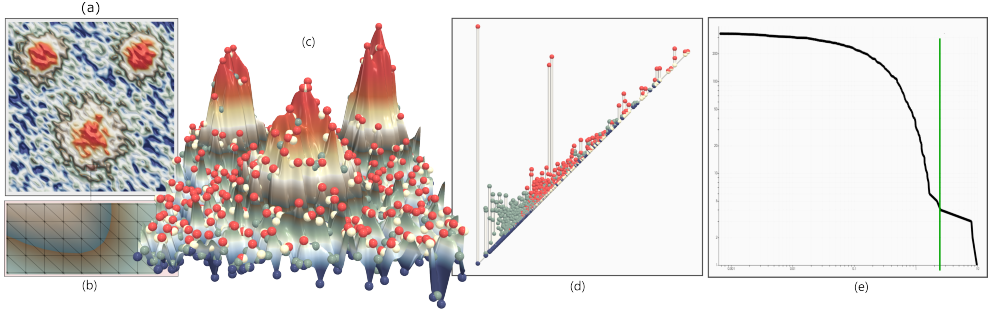
Figure 1. 2D noisy scalar field image (a). Scalar value interpolation at the vertices (b) of the grid. Terrain view of the image with critical points represented as spheres in blue for minima, white for saddles and red for maxima (c), The persistence diagram captures the main three hills of the terrain as prominent persistence pairs (large vertical segments), while small oscillations due to noise induce features near the diagonal (d). The persistence curve shows the number of persistent pairs as a function of their persistence. The green vertical line illustrates a persistence value which help to classifiy critical points between noise and persistence features (e).

2.2 Critical point

Topological features in f_i can be tracked with the notion of sub-level set noted $f_{i-\infty}^{-1}(w)$ and defined as the pre-image of $(-\infty, w)$ by f_i. The topology of this sub-level set can only change at special locations. As w continuously increases, the topology of the $f_{i-\infty}^{-1}(w)$ changes at specific vertices of $\mathcal{M}$, called the *critical points* of f_i [17]. The classification of the critical points can be done with a combinatorial approach by looking at the neighboring faces around a vertex. The *star* of a vertex $v \in \mathcal{M}$, noted $St(v)$, is the set of its co-faces: $St(v) = \{\sigma \in \mathcal{M} \mid v < \sigma\}$. It can be interpreted as the smallest combinatorial neighborhood around v. The *link* of v, noted $Lk(v)$, is the set of the faces τ of the simplices σ of $St(v)$ with empty intersection with v: $Lk(v) = \{\tau \in \mathcal{M} \mid \tau < \sigma, \sigma \in St(v), \tau \cap v = \emptyset\}$. The link of a vertex can be interpreted as the boundary of its star. The *lower link* of v, noted $Lk^-(v)$, is given by the set of simplices of $Lk(v)$ which only contain vertices *lower* than v and the upper link is defined symmetrically. A vertex v is *regular* if and only if both $Lk^-(v)$ and $Lk^+(v)$ are simply connected. For such vertices, the sub-level sets do not change their topology as they span $St(v)$. Otherwise, v is a *critical point* of f which can be classified as local minima ($Lk^-(v) = \emptyset$), as local maxima ($Lk^+(v) = \emptyset$) or saddles in all other cases as shown on Figure 1 (c).

2.3 Topological Persistence

Several importance measures for critical points have been studied such as the *topological persistence* [18]. Persistence assesses the importance of a critical point, based on the lifetime of the topological feature it created or destroyed in $f_{i-\infty}^{-1}(w)$, as the isovalue w continuously increases. [1] indicates that if two connected components, created at the minima m_0 and m_1 with $f_i(m_0) < f_i(m_1)$, meet at a given saddle s, the youngest of the two components (the one created at m_1) dies in favor of the oldest one (created at m_0). In this case, a persistence pair (m_1, s) is created and its *topological persistence p* is given by $p(m_1, s) = f_i(s) - f_i(m_1)$. All the local minima can be paired following this strategy, while the global minimum is usually paired, by convention, with the global maximum.

2.4 Persistence diagram

Persistence pairs are usually visualized with the *persistence diagram* [1], which embeds each pair (c, c'), with $f_i(c) < f_i(c')$, as a point in the 2D plane, at location $(f_i(c), f_i(c'))$ as shown on Figure 1(d). The value $f_i(c)$ is called the birth of the feature, while $f_i(c')$ is called its death. The pair persistence can be visualized as the height of the point to the diagonal. Features with a high persistence stand out, away from the diagonal, while noisy features are typically located in its vicinity. The persistence diagram is widely used during the analysis [18] because it summarizes the main features of interest and it is stable to perturbation such as additive noise.

2.5 Persistence curve

An interesting representation of persistence features is the *persistence curve*, which plots the number of persistent pairs as a function of their persistence as shown on Figure 1(e). In practice, large plateaus in this curve will indicate stable persistence ranges, for which no topological features are present in the data. The green vertical line on the Figure 1(e) illustrates a classification into the population of topological features usually caraterized as the noise for lower X values and persistence features for higher X values.

2.6 Wasserstein metric

To compare two datasets, persistence diagrams can be efficiently compared with the notion of L_2-Wasserstein distance [19]. The L_2-Wasserstein distance is based on a bipartite assignment optimization problem [20] between the points of the two diagrams to compare. It is defined as the minimal value achieved by an optimal matching between the points of the two diagrams and can be used for various comparisons [21]. .

2.7 Merge tree

The join tree is a graph-based representation which summaries the evolution of the connected components of $f_{i-\infty}^{-1}(w)$ [11]. Each leaf represents the creation or the deletion of a component while each interior vertex represents the joining or the splitting of components. An edge represents a component in the level sets for all values between the edge values. Symmetrically the split tree describes the connected components of the super-level set $f_{i+\infty}^{-1}(w)$. An interesting representation for segmentation can be created called the *merge tree* by combining the join tree (encoding the merges of components) with the split tree (encoding the splits of components).

2.8 Morse-Smale complex

The *Morse-Smale complex* is a topological representation that provides an abstract description of the gradient flow behavior of a scalar field [22]. It subdivides a given scalar field into regions of uniform gradient flow, segmenting the domain such that each point in the same Morse-Smale manifold will flow towards the same critical point pair. Several implementations are available [13] for more detail. The key concepts are based on a Morse function where all its critical points are non-degenerate and no two critical points have the same function value. An integral line in f is a path in $\mathcal{M}$ whose tangent vector agrees with the gradient of f at each point along the path. Ascending and descending manifolds are obtained as clusters of integral lines having common origin and destination respectively. The intersection of transversal ascending and descending manifolds of f defines the Morse-Smale complex segmentation.

3 Feature detection of Hydrodynamics Instabilities

Hydrodynamic instabilities [23] are a significant challenge in the development of Inertial Confinement Fusion (ICF) capsules. These instabilities arise during the convergence and implosion phases of the ICF process and have the potential to impede [24] the achievement of higher energy gains. As a result, dedicated Discovery Science campaigns [25] have been conducted at the world's largest laser facility, the National Ignition Facility (NIF), in order to gain a deeper understanding of the growth and possible control mechanisms of these detrimental instabilities. In particular, when starting from imprinted perturbations imposed by the laser focal spots, the ablative Rayleigh-Taylor instability gives birth at its highly nonlinear stage to complex three-dimensional patterns. In this work, we explore the radiographic images acquired during several experimental campaigns [9] on the NIF. Typical data analysis methods based on threshold and watershed segmentation [26] have been used to detect the peak-to-valley differences and the area of the bubbles. Such methods depend on parameters defined by the observers and may be enhanced. The idea is to evaluate several topological representations as introduced in Section 2 to provide novel segmentation techniques to help the scientists to identify bubble structures in the experimental campaign images.
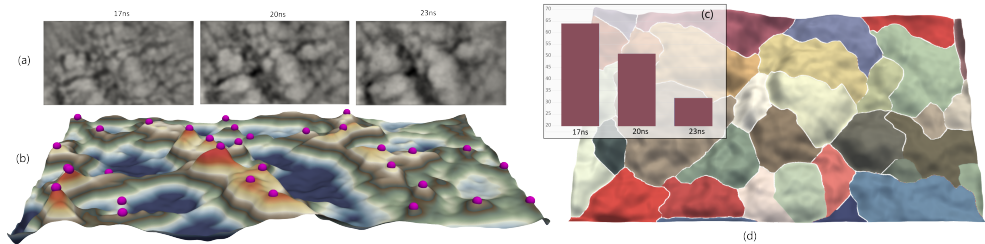
Figure 2. Radiographic images (a) from the N180213-001 dataset at 3 time steps shooted on the National Ignition Facility. Terrain view (b) of the 23 ns iteration showing the most persistent critical points corresponding to the the x-ray intensity maxima and minima. Topological segmentation (c) of the bubble region based on the separatrices of an ascending Morse-Smale complex simplified according to a persistence threshold. Distribution (c) of the number of features segmented by the Morse-Smale complex over time, confirming the decreasing number of bubbles into the hydrodynamic instability.

3.1 Data Description of radiography

We explored several dataset such as the NI180212 or NI180213 from the NIF. First, image processing on the raw data has been performed with different steps such as a backlighter reconstruction, a deconvolution and the calculation of a conversion factor from optical depth to physical units. Then ready-to-use x-ray images are interpreted as a scalar field and projected on a triangular mesh defining a manifold surface generated from the pixel structure. The size of experimental images of this study is 900×500.

3.2 TDA for Rayleigh-Taylor instability segmentation

As describe in [27], we iterated on the x-ray images shown on Figure 2 (*a*) to better understand the correlation between the pixel intensity and the bubble structure created during the development of the Rayleigh-Taylor instability at the interface between the two fluids. Then we use algorithms from the TDA to extract critical points as shown on Figure 2 (*b*) on the

x-ray intensity. The persistence as described in section 2.3 is computed and used to build a persistence diagram. Then a persistence threshold (0.2 in this study) is applied to keep all extrema pairs above and thus removed all pairs near the diagonal of the diagram. This treatment preserves the main structures in the x-ray images and remove small variations around bubbles. Then a Morse-Smale complex is computed as introduced in section 2.8 and shown in Figure 2 (*d*). We segment the x-ray by the 1-separatrices of the ascending Morse-Smale complex which leads to a very promising segmentation. To validate this segmentation, we compare the number of features segmented at each iteration 2 (*c*) and compare them with studies such as [28]. The Morse-Smale segmentation successfully capture the expected decreasing number of bubbles of the instability over time as shown on the histogram.

4 Vortex Segmentation in turbulent flows

Flow turbulence is an important phenomenon in fluid dynamics that engineers need to understand. The vortices produced by turbulent flow are difficult to analyze accurately due to their chaotic nature. Therefore, we decided to use topological analysis to segment vortices and their amplitude area to study turbulent flow.

4.1 Data Description from the simulation code

In order to segment vortices produced by turbulent flow, we used a compressible viscous testcase with a flow past two cylinders at Mach 0.425 and Reynolds number at 100000, at a final computational time $t = 80$. The data generated for the present study comes from a direct solver of the Navier-Stokes equations. The equations are solved using a conservative finite volume algorithm on a Cartesian grid [29] and complex geometry is handled using a ghost-cell based immersed boundary method [30]. To accurately compute turbulent flow, the approximate AUSM+up [31] solver has been used for the numerical fluxes, with the left and right states being interpolated using a 5th-order Weighted Essentially Non-Oscillatory Z (WENO-Z) scheme [32] and the Runge-Kutta third order scheme to compute time integration [33]. Reduce the number of parameters to a scalar field is crucial to be able to benefit from the TDA representation described in section 2. Thus we worked with a common measure to analyze turbulent flow which is the vorticity magnitude.
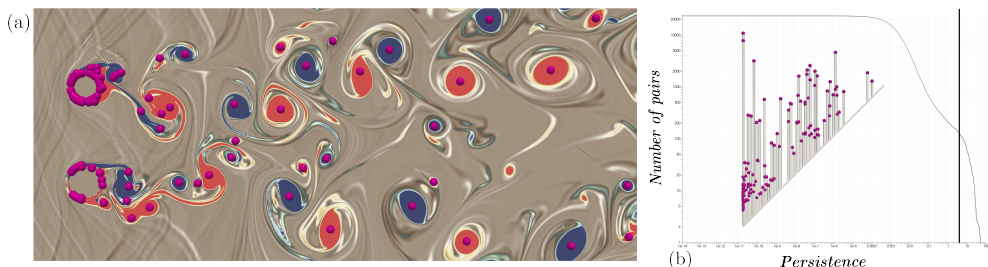

Figure 3. Vortices segmentation based on the direction rotation (a) computing on a grid 2000x400. Persistence diagram and persistence curve (b) for vorticity magnitude scalar field depending of a threshold represented as a vertical black line.

4.2 TDA for feature segmentation

To ease the segmentation of vortices various topological representations can be built on the vorticity magnitude scalar field. We first compute the persistence diagram and the persistence curve. To estimate an appropriate persistence threshold, we considered the persistence diagram which represents each minimum, denoting a vortex, as a vertical bar, whose height denotes the density amplitude of the vortex. Bars near the diagonal, corresponding to noisy structures, can easily be isolated (persistence below 4, represented in Figure 3) and the data can be simplified to account for this noise removal. Then a join tree is used for the vortex segmentation in order to identify the area of influence of such feature. The direction of rotation is then emphasized by changing the color of the segmentation based on the sign of the vorticity of the vortex (blue clockwise and red counter clockwise). With this representation we successfully segment and better understand the main features of the turbulent flow.

5 Comparison of ensembles for simulation code development

A multitude of numerical ingredients can be employed to simulate a given flow configuration, each of which is itself subject to a multitude of input parameters. These include domain resolution, methods of reconstruction, and solvers, among others. This leads to the generation of very large ensembles of data that post-processing techniques need to explore. In particular, domain experts are interested not only in identifying solver configurations that produce the most realistic simulations, but also in discovering configurations that result in degraded but fast computations, which still produce simulations of acceptable realism. It is evident that the correct selection of variables can result in a notable enhancement in the accuracy and efficiency of the experts' work, particularly in the context of turbulence, which is inherently a chaotic phenomenon. The objective of this study detailed in [34] is to demonstrate the potential of TDA to facilitate the identification of optimal numerical components that would otherwise be inaccessible through traditional fluid dynamics post-processing.
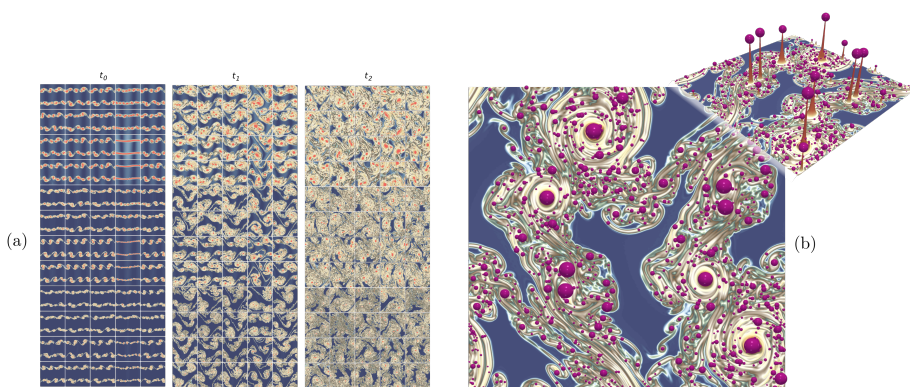
Figure 4. The 180 members of the ensemble (a) obtained with variations of timesteps, interpolation schemes, orders, resolutions and Riemann solvers. Top view (b) of one member with an elevation view showing extrema in the scalar field and critical points.
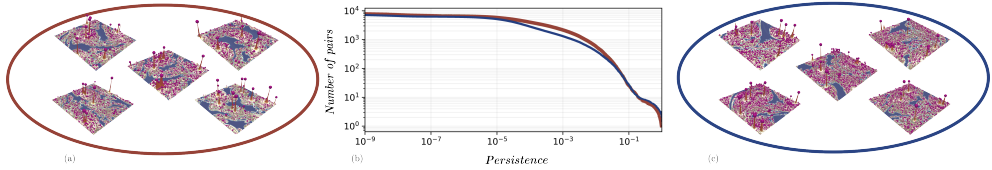
Figure 5. Terrain views of the TENO (a) and WENO-Z (c) scheme reconstruction for 5 different solvers. The average curves (b) represent the average persistence curve of all other solver configurations for the TENO in red and the WENO-Z in blue.

5.1 Data description of the ensemble

The simulation code considered is a two-dimensional compressible unsteady Euler equations for inviscid flows [29] with high-order low-dissipation reconstruction schemes of 5th- and 7th-order and a variety of Riemann solvers to evaluate the numerical fluxes between the cells. The development of such simulation code requires to evaluate lots of different combinations where the domain resolution, the simulation time, the interpolation scheme, the order of interpolation and the Riemann solvers can vary. To demonstrate the use of TDA on such data we consider a 2D turbulent instability generated with 5 parameters : Resolution: $256, 512, 1024$; Order: $5, 7$; Time: t_0, t_1, t_2; Solver [29]: HLL, SLAU2, AUSM+up, ROE, HLLC; Scheme: TENO [35], WENO-Z [32] leading to an ensemble of 180 members as shown on Figure 4 (a).

5.2 Scheme comparison with persistence curves

To demonstrate the correctness of TDA on such turbulent dataset, we state a known hypothesis based on the literature such that the TENO [35] scheme reconstruction presents more turbulence than the WENO-Z [32] no matter the other parameters are (resolution, time, solver). We therefore try to find a topological representations based on the critical points of the enstrophy scalar field which highlight this difference. The enstrophy is defined as the square of the flow vorticity : $\mathcal{E} = 0.5 |\nabla \times \mathbf{u}|^2$ with $\mathbf{u}$ the velocity vector. To better characterize all the vortices influencing the turbulence, we use persistence curves. These curves will allow us to threshold the vortices at different scales and use the integral of the persistence curves to take into account all the feature. The difference between two integral curves corresponds to our metric allowing to precisely describe the similarity in the topology of the critical points of the enstrophy. Bigger is the integral, the more different the topology of the instability is. Thus, to verify our hypothesis related to the differences between TENO and WENO-Z schemes, we want the difference of the integrals always different no matter the configurations of the solvers. Figure 5 shows the result of the study where the value of the difference between integrals is always different from 0. This same protocol has been used to different hypothesis such as the independence of order for certain solvers [34]. In this situation, with the exact same analysis workflow we confirmed the integral difference to be always close to 0 illustrating the relevance of the TDA approach for this numerical and physical description.

6 Conclusion

This work introduces several use cases of Topological Data Analysis to better understand the complex phenomena of instabilities and turbulences studied at CEA. This experience acquired on such chaotic data is useful for other applications and further work needs to be done

with even more meaningful topological representations. For example, the features of interest (bubbles in the x-ray images of hydrodynamic instablities or vortices in the turbulent flow) could be tracked over time with algorithms based on the distances between segmentations. Other promising topological distances [36] or clustering methods could also be evaluated depending on the physical phenomena to study.

References

[1] H. Edelsbrunner, J. Harer, *Computational Topology: An Introduction* (American Mathematical Society, 2009)

[2] J. Tierny, *Topological Data Analysis for Scientific Visualization* (Springer, 2018), ISBN 978-3-319-71507-0

[3] H. Edelsbrunner, J. Harer et al., *Persistent homology-a survey* (Providence, RI: American Mathematical Society, 2008), Vol. 453, pp. 257–282

[4] Y. Singh, C.M. Farrelly, Q.A. Hathaway, T. Leiner, J. Jagtap, G.E. Carlsson, B.J. Erickson, *Topological data analysis in medical imaging: current state of the art*, in *Insights Imaging* (2023), Vol. 14

[5] A. Gyulassy, P. Bremer, R. Grout, H. Kolla, J. Chen, V. Pascucci, *Stability of Dissipation Elements: A case study in combustion*, in *CGF* (2014)

[6] N. Shivashankar, P. Pranav, V. Natarajan, R. van de Weygaert, E.P. Bos, S. Rieder, *Felix: A Topology Based Framework for Visual Exploration of Cosmic Filaments* (IEEE, 2016)

[7] C. Heine, H. Leitte, M. Hlawitschka, F. Iuricich, L. De Floriani, G. Scheuermann, H. Hagen, C. Garth, *A Survey of Topology-based Methods in Visualization*, in *CGF* (2016)

[8] T. Günther, I. Baeza Rojo, in *Topological Methods in Data Analysis and Visualization VI* (Springer, 2021)

[9] L. Ceurvorst, S. Khan, C. Mailliet, D. Martinez, N. Izumi, P.D. Nicola, J.D. Nicola, T. Goudal, V. Bouffetier, D. Kalantar et al., *Post-processing of face-on radiographic images for quantitative analysis in ablative Rayleigh-Taylor instability experiments* (Elsevier, 2020), Vol. 37, p. 100851, ISSN 15741818

[10] J. Kasten, J. Reininghaus, I. Hotz, H. Hege, *Two-dimensional time-dependent vortex regions based on the acceleration magnitude*, in *IEEE TVCG* (2011)

[11] H. Carr, J. Snoeyink, U. Axen, *Computing contour trees in all dimensions*, in *Symp. on Dis. Alg.* (2000)

[12] H. Edelsbrunner, J. Harer, A. Zomorodian, *Hierarchical morse complexes for piecewise linear 2-manifolds*, in *SoCG* (2001)

[13] A. Gyulassy, P. Bremer, V. Pascucci, *Shared-Memory Parallel Computation of Morse-Smale Complexes with Improved Accuracy* (2018)

[14] L. Yan, T.B. Masood, R. Sridharamurthy, F. Rasheed, V. Natarajan, I. Hotz, B. Wang, *Scalar Field Comparison with Topological Descriptors: Properties and Applications for Scientific Visualization* (2021)

[15] J. Ahrens, B. Geveci, C. Law, *ParaView: An End-User Tool for Large-Data Visualization*, in *The Visualization Handbook* (Academic Press, Inc., 2005), pp. 717–731

[16] J. Tierny, G. Favelier, J.A. Levine, C. Gueunet, M. Michaux, *The Topology ToolKit*, in *IEEE Transactions on Visualization and Computer Graphics (Proc. of IEEE VIS)* (2017), https://topology-tool-kit.github.io

[17] T.F. Banchoff, *Critical Points and Curvature for Embedded Polyhedral Surfaces* (1970)

[18] H. Edelsbrunner, D. Letscher, A. Zomorodian, *Topological Persistence and Simplification* (2002)

[19] D. Cohen-Steiner, H. Edelsbrunner, J. Harer, *Stability of persistence diagrams*, in *SoCG* (2005)

[20] J. Munkres, *Algorithms for the Assignment and Transportation Problems*, in *Journal of the Society of Industrial and Applied Mathematics* (1957), Vol. 5, pp. 32–38

[21] J. Vidal, J. Budin, J. Tierny, *Progressive Wasserstein Barycenters of Persistence Diagrams*, in *IEEE TVCG* (2019)

[22] H. Edelsbrunner, J. Harer, A. Zomorodian, *Hierarchical Morse-Smale Complexes for Piecewise Linear 2-Manifolds* (2003)

[23] A. Casner, *Recent progress in quantifying hydrodynamics instabilities and turbulence in inertial confinement fusion and high-energy-density experiments*, in *Philosophical Transactions of the Royal Society A* (The Royal Society Publishing, 2021), Vol. 379

[24] G.H. McCall, *Cloud and microjet mix: A possible source of yield limitation of the National Ignition Facility targets*, in *Physics of Plasmas* (AIP Publishing, 2023), Vol. 30

[25] A. Casner, V. Smalyuk, L. Masse, I. Igumenshchev, S. Liberatore, L. Jacquet, C. Chicanne, P. Loiseau, O. Poujade, D. Bradley et al., *Designs for highly nonlinear ablative Rayleigh-Taylor experiments on the National Ignition Facility*, in *Physics of Plasmas* (AIP Publishing, 2012), Vol. 19

[26] O. Sadot, V.A. Smalyuk, J.A. Delettrez, D.D. Meyerhofer, T.C. Sangster, R. Betti, V.N. Goncharov, D. Shvarts, *Observation of Self-Similar Behavior of the 3D, Nonlinear Rayleigh-Taylor Instability*, in *Phys. Rev. Lett.* (American Physical Society, 2005)

[27] F. Vivodtzev, A. Casner, L. Masse, L. Ceurvorst, S. Khan, V. Smalyuk, *Poster: Topological Data Analysis of 3D Ablative Rayleigh-Taylor Instability Dataset for Automatic Segmentation*, in *The 13th IEEE Symposium on Large Data Analysis and Visualization, LDAV 2023* (2023)

[28] C. Mailliet, Etude expérimentale et numérique du stade fortement non-linéaire de l'Instabilité de Rayleigh-Taylor au front d'ablation en attaque directe, Doctoral dissertation of the Université de Bordeaux (2018)

[29] E.F. Toro, *Riemann solvers and numerical methods for fluid dynamics: a practical introduction* (Springer Berlin Heidelberg, 2009)

[30] T. Bridel-Bertomeu, *Immersed boundary conditions for hypersonic flows using ENO-like least-square reconstruction*, in *Computers and Fluids* (2020), Vol. 215

[31] M.S. Liou, *A sequel to AUSM, Part II: AUSM+-up for all speeds*, in *Journal of computational physics* (Elsevier, 2006), Vol. 214, pp. 137–170

[32] M. Castro, B. Costa, W.S. Don, *High order weighted essentially non-oscillatory WENO-Z schemes for hyperbolic conservation laws*, in *Journal of Computational Physics* (Elsevier, 2011), Vol. 230, pp. 1766–1792

[33] S. Gottlieb, C.W. Shu, *Total variation diminishing Runge-Kutta schemes*, in *Mathematics of computation* (1998), Vol. 67, pp. 73–85

[34] F. Nauleau, F. Vivodtzev, T. Bridel-Bertomeu, H. Beaugendre, J. Tierny, *Topological Analysis of Ensembles of Hydrodynamic Turbulent Flows – An Experimental Study*, in *Proc. of IEEE Symposium on Large Data Analysis and Visualization* (2022)

[35] L. Fu, X.Y. Hu, N.A. Adams, *A family of high-order targeted ENO schemes for compressible-fluid simulations*, in *Journal of Computational Physics* (Elsevier, 2016), Vol. 305, pp. 333–359

[36] M. Pont, J. Vidal, J. Delon, J. Tierny, *Wasserstein Distances, Geodesics and Barycenters of Merge Trees* (2021)